Nuclear Instruments and Methods in Physics Research B 268 (2010) 3009–3013

Contents lists available at ScienceDirect

Nuclear Instruments and Methods in Physics Research B

journal homepage: www.elsevier.com/locate/nimb

Damage evolution in Au-implanted $Ho_2Ti_2O_7$ titanate pyrochlore

Yanwen Zhang [a,*], Jacek Jagielski [b,c], In-Tae Bae [d], Xia Xiang [e], Lionel Thomé [f], Geetha Balakrishnan [g], Don M. Paul [g], William J. Weber [a]

[a] Pacific Northwest National Laboratory, Richland, WA 99352, USA
[b] Institute for Electronic Materials Technology, Wolczynska 133, 01-919 Warsaw, Poland
[c] The Andrzej Soltan Institute for Nuclear Studies, 05-400 Swierk/Otwock, Poland
[d] Small Scale Systems Integration and Packaging Center, State University of New York at Binghamton, P.O. Box 6000, Binghamton 13902, USA
[e] University of Electronic Science and Technology of China, Chengdu, People's Republic of China
[f] Centre de Spectrométrie Nucléaire et de Spectrométrie de Masse, CNRS-IN2P3-Université Paris Sud,UMR 8609, Bât. 108, 91405 Orsay, France
[g] Department of Physics, University of Warwick, Coventry CV4 7AL, UK

ARTICLE INFO

Article history:
Received 21 September 2009
Received in revised form 2 April 2010
Available online 7 May 2010

Keywords:
Damage accumulation
Amorphization
Holmium titanate pyrochlore
Irradiation
Rutherford backscattering spectroscopy

ABSTRACT

Damage evolution at room temperature in $Ho_2Ti_2O_7$ single crystals is studied under 1 MeV Au^{2+} ion irradiation by Rutherford backscattering spectroscopy along the ⟨0 0 1⟩ direction. For a better determination of ion-induced disorder profile, an iterative procedure and a Monte Carlo code (McChasy) were used to analyze ion channeling spectra. A disorder accumulation model, with contributions from the amorphous fraction and the crystalline disorder, is fit to the Ho damage accumulation data. The damage evolution behavior indicates that the relative disorder on the Ho sublattice follows a nonlinear dependence on dose and that defect-stimulated amorphization is the primary amorphization mechanism. Similar irradiation behavior previously was observed in $Sm_2Ti_2O_7$. A slower damage accumulation rate for $Ho_2Ti_2O_7$, as compared with damage evolution in $Sm_2Ti_2O_7$, is mainly attributed to a lower effective cross section for defect-stimulated amorphization.

1. Introduction

Pyrochlore materials, due to the remarkable elemental versatility in the $A_2B_2O_7$ crystal structure, are considered for a wide range of applications, such as fuel cells [1,2], catalysts [3,4], and immobilization of actinide-rich nuclear waste [5–7] or excess plutonium [8,9] Considerable self-radiation damage from alpha decay in actinide-bearing phases can result in amorphization, macroscopic swelling and order-of magnitude increase in dissolution rates [10–13], and these changes in structure and chemical durability affect long-term performance of the actinide waste forms [9–15]. Studies of actinide-doped [11,12,16] and natural pyrochlores [17], indicate that pyrochlores with Ti, Nb, and Ta as the major B-site cations become amorphous as a result of the gradual accumulation of alpha-recoil collision cascades. However, such studies are time consuming, and only limited data under a few sets of experimental conditions are available. Heavy-ion irradiation studies [6,13,18–28] have been used to more rapidly evaluate radiation effects on a wide range of pyrochlore compositions that generally confirm the results for the actinide-doped pyrochlores or natural minerals.

In general, alpha decay of actinide elements produces high-energy alpha particles and low-energy heavy recoil nuclei (alpha recoils) [15]. The alpha particles with energies of 4.5–5.8 MeV, due to smaller mass, have relatively less radiation impact. The heavy recoil nuclei (alpha recoils) with energies of 70–100 keV account for most of the crystal damage produced through elastic scattering collisions. Since nuclear stopping at the damage peak resulting from heavy-ion irradiation, such as Au ion, is similar to the nuclear stopping of alpha recoils (~5 keV/nm), the damage evolution at the damage peak under heavy-ion irradiation provides a reasonable simulation of the damage evolution behavior due to alpha-recoil collision cascades. Accumulation of alpha decay damage may lead to serious disorder or even a crystalline to amorphous transition. Such phase transformation may enhance the ceramic aqueous dissolution and produce a large swelling leading to cracks or even fragmentation of the waste form. Since both effects may increase the actinide release, it is important to understand and predict the behavior of the pyrochlore materials in a radiation environment.

Considerable transmission electron microscope (TEM) studies have been carried out to characterize the temperature dependence of the critical dose for amorphization [6,13,24–28], few studies have quantitatively investigated the damage evolution behavior as a function of irradiation dose [20–23] at different temperatures, particularly in relevant pyrochlore phases. In this work, quantitative characterization of damage accumulation in holmium titanate

* Corresponding author.
E-mail address: Yanwen.Zhang@pnl.gov (Y. Zhang).

0168-583X/$ - see front matter © 2010 Elsevier B.V. All rights reserved.
doi:10.1016/j.nimb.2010.05.029

($Ho_2Ti_2O_7$) single crystals as a function of irradiation dose is carried out using ion-channeling methods, which should lead to a better understanding of the amorphization and damage evolution processes.

2. Experimental procedures

The $Ho_2Ti_2O_7$ single crystals used in current work were grown by a floating zone technique using an infrared image furnace at the University of Warwick, UK [29]. The pyrochlore crystal was sectioned along the (1 0 0) plane. The polished samples were characterized by high-resolution X-ray diffraction (HRXRD) and a series of pole figure measurements. Samples exhibiting large single crystal regions were then selected for the irradiation experiments. Some material was crushed for powder XRD, which revealed no evidence for the existence of secondary or minor phases.

The Au irradiations and subsequent ion beam analysis of damage accumulation in the $Ho_2Ti_2O_7$ single crystals were carried out using the 3.0 MV tandem accelerator facility within Environmental Molecular Sciences Laboratory (EMSL) at the Pacific Northwest National Laboratory (PNNL). Each sample was mechanically mounted to a molybdenum plate using molybdenum spring-loaded clips, with a chromel–alumel thermocouple clamped to the sample surface. The samples were irradiated with 1.0 MeV Au^{2+} ions at 300 K 7° off the ⟨0 0 1⟩ direction. The ion fluences are chosen from 2×10^{12} to 3.1×10^{13} Au^+ cm^{-2}, which produced damage states that ranged from relatively minor disorder to a fully amorphous layer. The beam energy was chosen to produce shallow damage that could be readily measured by the ion channeling technique. For each ion fluence, the local dose at the damage peak, in displacements per atom (dpa), was determined using the Stopping and Range of Ions in Matter (SRIM) 2008 code [30]] under full-cascade mode, assuming a theoretical density of 6.926 g/cm^3 and threshold displacement energies of 50 eV for Ho, Ti and O atoms [10]. The conversion factor at the damage peak from ion fluence (10^{14} Au^+ cm^{-2}) to dose (dpa) is 0.438 under the irradiation conditions of this study.

The damage evolution was investigated by the relative disorder determined by backscattering spectroscopy (RBS) along the ⟨0 0 1⟩ channel direction. Helium ions of 2.0 MeV were used as probing beam and the backscattering angle was 150°. Energy calibration of E (keV) = E (ch) × 2.045 (keV/ch) + 71.4 (keV) is used to convert to an energy spectrum. For ion-beam induced damage, the backscattering yield is primarily due to interstitials within channels, unaligned atoms in amorphous domains, and unaligned atoms due to local strain from dislocations. The ion-channeling methods are not as sensitive to vacancies, antisite defects, or the cation and anion disorder; however, the influence of such defects may be noticeable by the increase of dechanneling fraction. The disordering measured in the present study by ion channeling is disorder associated with anions and cations on non-crystalline sites.

3. Results and discussion

3.1. Damage accumulation

Channeling RBS spectra for the irradiated samples along the ⟨1 0 0⟩ direction in $Ho_2Ti_2O_7$ are shown in Fig. 1. For clarity purpose, only the result from ion fluences of 9×10^{12}, 1.5×10^{13}, 2.1×10^{13}, 2.7×10^{13} cm^{-2} are included, which illustrates the general statistics for other irradiated samples. The random and channeling spectra from a virgin area are also included to indicate the fully amorphous and essentially defect-free states, respectively. The ratio of the backscattering yield in the virgin spectrum to the yield in the random spectrum just below the surface peak, χ_{min}, is ~3.7%, which indicates the good quality of the crystal. The emergence of the damage peaks in the channeling spectra indicates the presence of disorder that causes backscattering of the channeled ions. As shown in Fig. 1, the increase in disorder on the Ho and Ti sublattices with increasing ion fluences is evident. Because the damage accumulation starts from the surface and increases with ion fluence, the surface peak cannot be resolved.

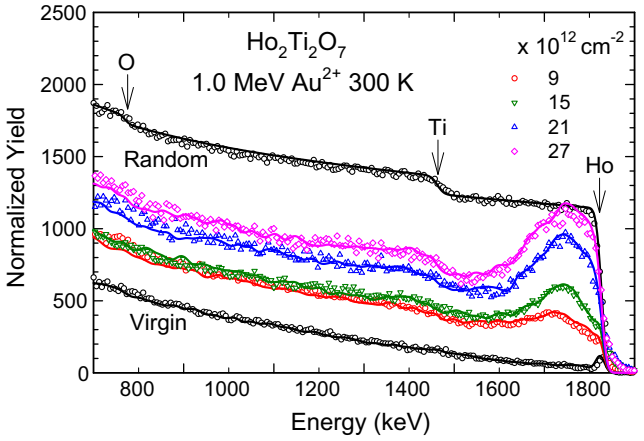

Fig. 1. A series of ⟨1 0 0⟩- aligned RBS spectra for $Ho_2Ti_2O_7$ samples under 1.0 MeV Au irradiation at room temperature to ion fluences from 9×10^{12} to 2.7×10^{13} cm^{-2}. Random and channeling spectra from a virgin area are also included. For clarity purpose, every three data points are shown. Backscattered He ions from the sample surface are marked for the Ho, Ti and O sublattices, respectively. The lines are the simulation results from the McChasy code.

In order to obtain a quantitative damage profile, an iterative procedure [31–35] is applied to determine the dechanneling component of the RBS spectra as a function of depth. Because the backscattering yield due to the ion-beam-induced disordering is much more evident from the Ho sublattice, all analyses of cation disordering were performed on that part of the spectrum. For each ion fluence, a set of three spectra is needed to determine the corresponding disorder profile: the measured channeling spectra from both the irradiated sample and the virgin sample, as well as the random spectrum [32]. Both the normalized spectra, $V(x)$ and $\eta(x)$, from the virgin spectrum and the damaged spectrum can be achieved by normalizing the corresponding channeling spectra to the random spectrum. The dechanneling component, $R(x)$, starts from a point, x_0, on the normalized virgin spectrum near the beginning of the damaged region, where the dechanneling component $R(x_0)$ is assumed to be zero.

$$R(x) = V(x) + [1 - V(x)] \times \left(1 - \exp\left[-\sigma_D \times \sum_{x+1}^{x_0}\left[\left(\frac{\eta(x+1) - R(x+1)}{1 - R(x+1)}\right)\right]\right]\right) \quad (1)$$

The iterative procedure [32] successively moves in depth to the next channel, as described in Eq. (1), to determine the dechanneling function, $R(x)$, which enables the separation of the direct backscattering contribution from the displaced atoms at that depth. The parameter, σ_D, is the only adjustable parameter that is related to dechanneling cross section for the disorder along the axial channel direction, and can be determined when the dechanneling component $R(x)$ overlaps with the normalized channeling spectrum $\eta(x)$ after the damage peak. After separation of the dechanneling component from the direct backscattering contribution, $\eta(x) - R(x)$, the profile of the relative Ho disorder is then derived by $[\eta(x) - R(x)]/[1 - R(x)]$. The continuous amorphous state determined by RBS corresponds to a relative disorder level of 1.0, where the aligned spectrum overlaps with the random spectrum.

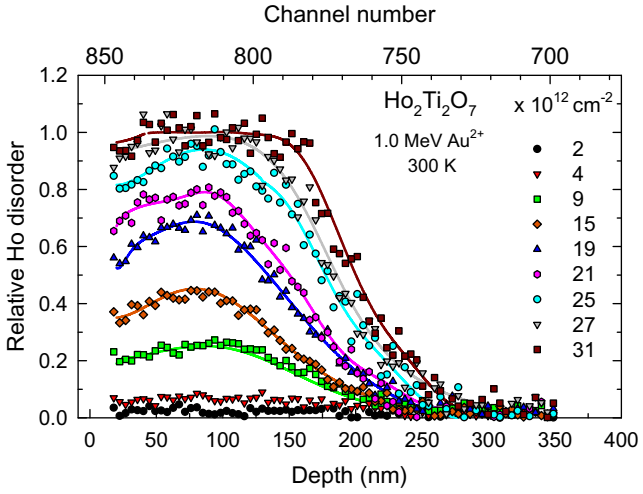

Fig. 2. Disorder profiles on the Ho sublattice of the $Ho_2Ti_2O_7$ samples after irradiation to different ion fluences from 2×10^{12} to 3.1×10^{13} cm^{-2}. For clarity purpose, every two data points are shown.

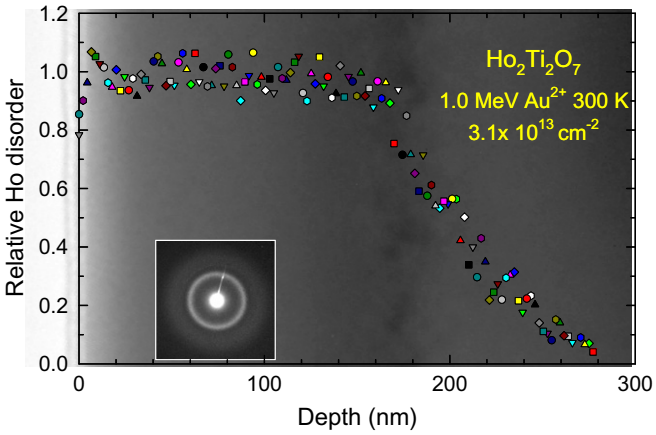

Fig. 3. The damage profile of $Ho_2Ti_2O_7$ irradiated with 1 MeV Au^+ at 300 K to an ion fluence of 3.1×10^{13} cm^{-2}. The profile, measured by channeling RBS and analyzed from the iterative procedure, is overlaid on the corresponding TEM image. Also included as inset is SAED pattern taken from the region where it locates.

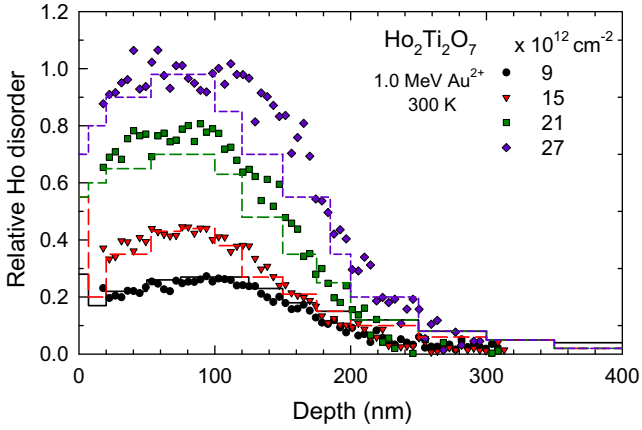

Fig. 4. Comparisons of the disorder profiles on the Ho sublattice after irradiation to different ion fluences of 9×10^{12}, 1.5×10^{13}, 2.1×10^{13} and 2.7×10^{13} cm^{-2}. The data points indicate the results analyzed from the iterative procedure, and the lines are the simulation results from the McChasy code. For clarity purpose, every two data points are shown.

The disorder profiles on the Ho sublattice under irradiation fluences from 2×10^{12} to 3.1×10^{13} have been determined using the iterative procedure, and the results are summarized in Fig. 2. The depth scale in nm is determined by the energy difference at each channel and the He ion stopping in $Ho_2Ti_2O_7$ from the SRIM 2008 simulations [30] under the assumptions of a sample density of 6.926 g/cm^3 (8.533×10^{22} at cm^{-3}). Stopping powers of helium ions have been experimentally measured in a few compounds over the energy region that is of interests for RBS measurement [36–41]. Good agreements with the SRIM predictions provide some confidence of using the SRIM predicted He stopping in $Ho_2Ti_2O_7$. The stopping powers of He in the aligned directions are assumed to be the same as in the random direction in the current study, since channeling influence is negligible. As ion fluence increases, the disorder increases over the whole irradiation depth, eventually achieving a buried amorphous state after irradiation to 2.7×10^{13} cm^{-2}. Further irradiation results in a buried amorphous layer that expands toward the surface and deeper into the bulk. To confirm the amorphous state, the sample has been characterized by TEM, and the damage profile of the sample irradiated to the highest ion fluence (3.1×10^{13} cm^{-2}) measured by channeling RBS is overlaid on the corresponding bright-field (BF) TEM image in Fig. 3. The amorphous nature of the material is clearly shown by the selected-area electron diffraction (SAED) patterns taken from the corresponding area. Good correlation is shown between the location of the amorphous/crystalline interface and the width of the RBS profiles, where the 100% disorder region from the damage profile overlaps with the no-contrast region in the BF TEM image.

The disorder profile can also be obtained from a Monte Carlo code (McChasy) [42] that is used to directly simulate ion channeling spectra. The fitting results of the backscattering yield by assuming randomly displaced atoms are shown by the lines in Fig. 1, and good agreement is evident. The resulting damage profiles (depth distribution of the equivalent scattering centers) are shown in Fig. 4 as lines, together with the results from the iterative procedure indicated by points. Good agreement between the relative disorder profiles resulting from the iterative procedure and the McChasy simulation suggests that both analysis methods can be applied to the irradiated samples in this study. The iterative procedure is easy and fast, if the damage peak is close to the surface, and interference with backscattering yield from other target elements is insignificant so that σ_D can be determined, as the case in this study and in previous studies [31,32]. The McChasy simulation requires constructing target structure, and long simulation time. However, the damage profile of light element sublattice may be determined with better accuracy than the iterative procedure. Furthermore, in some materials or under certain irradiation conditions, when dislocation loops cannot be ignored, the McChasy simulation can provide the information on amount and depth distribution of the dislocation loops as well as the randomly displaced target atoms. The McChasy code can also be used to fit the RBS spectra of the samples irradiated to high energies, where the damage peak is not visible from the RBS channeling spectra [43], or to the analysis of multi-elemental targets where an overlap of numerous elemental contributions makes standard analysis difficult.

3.2. Defect-stimulated amorphization

Several amorphization models and mechanisms have been discussed in a detailed review [44] to quantitatively characterize damage evolution. A disorder accumulation model is used in this study. In this model, the measured irradiation-induced relative disorder, S, contains contributions from amorphous material, interstitials, interstitial clusters and extended defects, and is described by the expression [22,45–47].

$$S = f_a + S_d + S_c \quad (2)$$

where f_a is the amorphous fraction, and S_d is the relative disorder contribution from interstitials and small interstitial clusters in the residual crystalline material. The third term, S_c, accounts for the relative disorder from the growth of extended defect clusters or dislocation loops, which may be a significant contribution at irradiation temperatures close to the critical temperature for amorphization [47], where point defects are more mobile. Under the current study, the contribution of S_c to the total disorder is insignificant at 300 K in $Ho_2Ti_2O_7$. This is confirmed by the good fit of the McChasy simulation to the experimental spectra in Fig. 1, where the disorder is assumed to be randomly displaced atoms. Therefore, contribution from S_c will not be discussed further.

The amorphous fraction can be described using a direct-impact, defect-stimulated (DI/DS) model for amorphization [44]. In this model, amorphous nuclei are directly produced in the core of a cascade, and the irradiation-induced point defects accumulate and stimulate further amorphization at the crystalline–amorphous interfaces. An analytical solution for the amorphous fraction, where amorphization occurs both directly within a cascade and from defect-stimulated processes, is given by an expression [44],

$$f_a = 1 - (\sigma_a + \sigma_s)/\{\sigma_s + \sigma_a \exp[(\sigma_a + \sigma_s)D]\}, \quad (3)$$

where σ_a is the amorphization cross section, σ_s is the effective cross section for defect-stimulated amorphization, and D is the local dose (dpa). The relative disorder, S_d, is primarily due to the accumulation of interstitial defects in the residual crystalline material that can be described using a simple defect accumulation model [20,46–49],

$$S_d = S_d^*[1 - \exp(-BD)](1 - f_a), \quad (4)$$

where S_d^* is the saturation value for the defect-induced disorder observed along a specified channel direction; and B (dpa^{-1}) is proportional to an effective recombination volume for the specific defects giving rise to S_d.

The relative disorder at the damage peak on the Ho sublattice in $Ho_2Ti_2O_7$ at 300 K is shown in Fig. 5 as a function of the local dose in dpa. The results show that the atomic disorder increases nonlinearly with dose, approaching a fully amorphous state at doses of ~0.12 dpa. The curves shown in Fig. 5 are fits of the above model [Eqs. (2)–(4)] to the experimental results, and the model parameters are summarized in Table 1. The contributions from the local amorphous regions (f_a) and crystalline domains (S_d) to the total disorder are given in the plot to help the discussion. At low doses, the defect-related disorder (S_d) is important. As the irradiation dose increases (> ~ 0.03 dpa), the amorphous fraction (f_a) becomes significant. Furthermore, since the crystalline fraction ($1 - f_a$) decreases as a result of the increasing amorphous fraction, the contribution from the defect disorder (S_d) eventually becomes negligible above 0.1 dpa. There may be considerable uncertainty in these fit parameters at this time due to the limited data for the pyrochlore system, but it is expected that the uncertainty will be reduced as more experimental data are obtained and analyzed, as was demonstrated for SiC [46,47]. The significantly larger value of σ_s relative to σ_a, as shown in Table 1, indicates that defect-stimulated amorphization is the primary mechanism that leads to the growth of amorphous nuclei and coalescence of amorphous domains in

Table 1
Model parameters from fits of Eqs. (2)–(4) to data in Figs. 5 and 6.

	Ho sublattice	Sm sublattice
σ_a (dpa^{-1})	1.0	1.0
σ_s (dpa^{-1})	56.8	66.0
S_d^*	0.25	0.28
B (dpa^{-1})	10	10

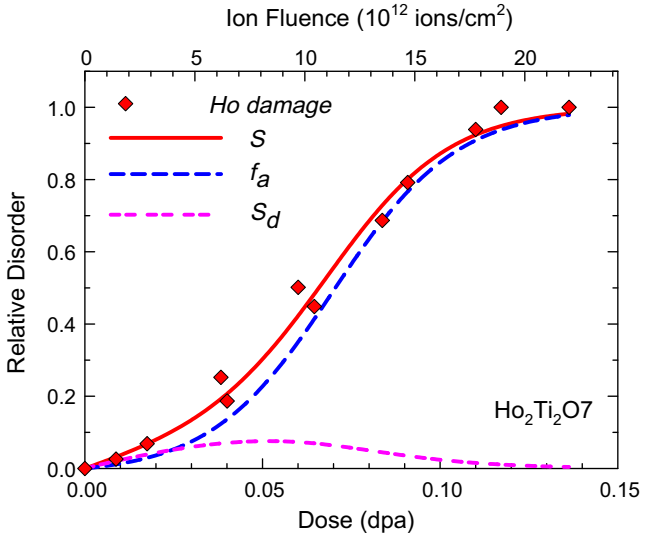

Fig. 5. Relative disorders at the damage peak on the Ho sublattice as a function of local dose for $Ho_2Ti_2O_7$ single crystals implanted with 1.0 MeV Au^+ at 300 K. Solid line is the fit of the total disorder (S) to the data using Eqs. (3) and (4). The contributions from the amorphous fraction (f_a) and the relative disorder from irradiation-induced interstitials and clusters (S_d) are also indicated.

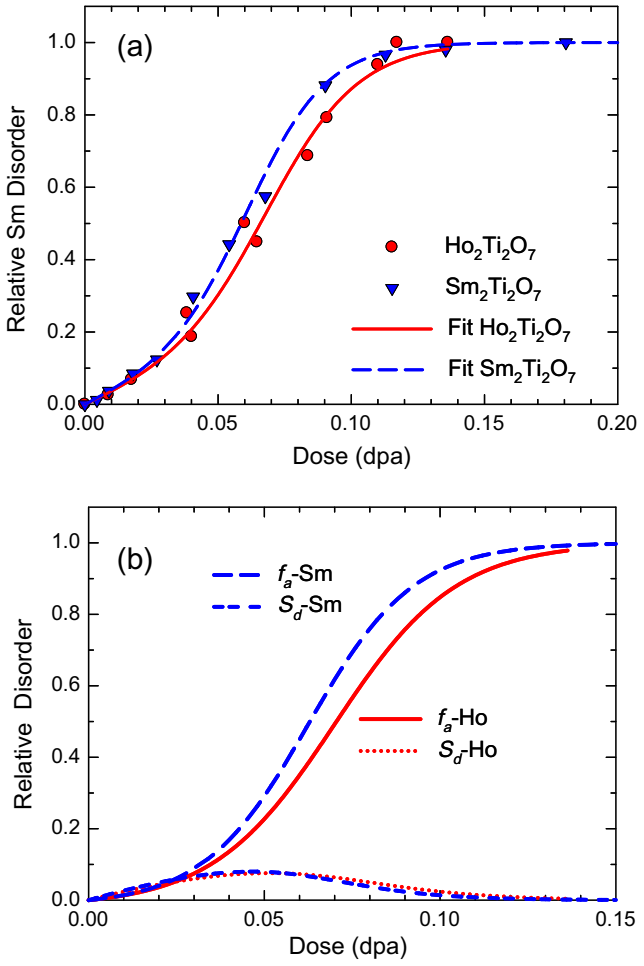

Fig. 6. Comparison of damage accumulation behaviors for $Ho_2Ti_2O_7$ and $Sm_2Ti_2O_7$ single crystals implanted with 1.0 MeV Au^+ at 300 K, (a) fits of the total disorder (S) to the data points, and (b) the contributions from f_a and S_d.

$Ho_2Ti_2O_7$, which is similar to the irradiation behavior previously observed in $Sm_2Ti_2O_7$ [22], as shown in Fig. 6. The contributions from S_d in Fig. 6(b) to the total disorder are similar in both $Ho_2Ti_2O_7$ and $Sm_2Ti_2O_7$ materials. A slower observed damage accumulation rate for $Ho_2Ti_2O_7$, as compared with damage evolution in $Sm_2Ti_2O_7$, is mainly attributed to a lower effective cross section (σ_s) for defect-stimulated amorphization, 57 dpa^{-1} for the Ho sublattice and 66 dpa^{-1} for the Sm sublattice. The quantitative details on the damage accumulation processes, as shown in Figs. 5 and 6, provide a better understanding of the defects and amorphization mechanism, which has not been obtained in TEM studies, to assess the impact of alpha decay events on long-term performance.

4. Conclusions

Using single crystals of $Ho_2Ti_2O_7$, the damage evolution on the Ho sublattice under 1.0 MeV Au irradiation is characterized at 300 K using channeling RBS technique along the ⟨0 0 1⟩ direction. For a better determination of ion-beam-induced disorder profile, the iterative procedure and the McChasy code were applied to analyze the ion channeling spectra. The results show that the atomic disorder on the Ho sublattice increases nonlinearly with ion dose, eventually achieving a fully amorphous state. The disorder accumulation model was employed to characterize the defect accumulation and amorphization behavior, and the result indicates a significant role of defect-stimulated amorphization processes. A slower damage accumulation rate for $Ho_2Ti_2O_7$, as compared with damage evolution in $Sm_2Ti_2O_7$, is mainly attributed to a lower effective cross section for defect-stimulated amorphization.

Acknowledgements

This work was supported by the US Department of Energy, Office of Basic Energy Sciences. Ion beam work and TEM observation were performed in EMSL, a national scientific user facility sponsored by the Department of Energy's Office of Biological and Environmental Research and located at Pacific Northwest National Laboratory. Pacific Northwest National Laboratory is operated by Battelle for the U.S. Department of Energy under Contract No. DE-AC05-76RL01830.

References

[1] H.L. Tuller, J. Phys. Chem. Solids 55 (1994) 1393.
[2] B.J. Wuensch, K.W. Eberman, C. Heremans, E.M. Ku, P. Onnerud, E.M.E. Yeo, S.M. Haile, J.K. Stalick, J.D. Jorgensen, Solid State Ionics 129 (2000) 111.
[3] J.B. Goodenough, R.N. Castellano, Solid State Chem. 44 (1982) 109.
[4] S.J. Korf, H.J.A. Koopmans, B.C. Lippens, A.J. Burggraaf, P.J. Gellings, J. Chem. Soc. Faraday Trans. 83 (1987) 1485.
[5] K.E. Sickafus, L. Minervini, R.W. Grimes, J.A. Valdez, M. Ishimaru, F. Li, K.J. McClellan, T. Hartmann, Science 289 (2000) 748.
[6] S.X. Wang, B.D. Begg, L.M. Wang, R.C. Ewing, W.J. Weber, K.V. Govidan Kutty, J. Mater. Res. 14 (1990) 4470.
[7] W.J. Weber, A. Navrotsky, S. Stefanovsky, E.R. Vance, E. Vernaz, Materials Science of High-Level Nuclear Waste Immobilization, MRS Bull. 34 (2009) 46.
[8] B.R. Myers, G.A. Armantrout, C.M. Jantzen, A. Jostsons, J.M. McKibben, H.F. Shaw, D.M. Strachan, J.D. Vienna, Technical Evaluation Panel Summary Report, Plutonium Immobilization Project, Report No. UCRL-ID-129315 (1998).
[9] R.C. Ewing, W.J. Weber, W. Lutze, in: E.R. Merz, C.E. Walter (Eds.), Diposal of Weapon Plutonium, Kluwer Academic Publishers., The Netherlands, 1996, p. 65.
[10] B.D. Begg, N.J. Hess, W.J. Weber, R. Devanathan, J.P. Icenhower, S. Thevuthasan, B.P. McGrail, J. Nucl. Mater. 288 (2001) 208.
[11] W.J. Weber, J.W. Wald, Hj. Matzke, Mater. Lett. 3 (1985) 173.
[12] W.J. Weber, J.W. Wald, Hj. Matzke, J. Nucl. Mater. 138 (1986) 196.
[13] B.D. Begg, W.J. Weber, R. Devanathan, J.P. Icenhower, S. Thevuthasan, B.P. McGrail, Ceram. Trans. 107 (2000) 553.
[14] R.C. Ewing, W.J. Weber, F.W. Clinard Jr., Prog. Nucl. Energy 29 (1995) 63.
[15] W.J. Weber, R.C. Ewing, C.R.A. Catlow, T. Diaz de la Rubia, L.W. Hobbs, C. Kinoshita, Hj. Matzke, A.T. Motta, M. Nastasi, E.K.H. Salje, E.R. Vance, S.J. Zinkle, J. Mater. Res. 13 (1998) 1434.
[16] D.M. Strachan, R.D. Scheele, E.C. Buck, J.P. Icenhower, A.E. Kozelisky, R.L. Sell, R.J. Elovich, W.C. Buchmiller, J. Nucl. Mater. 345 (2005) 109.
[17] G.R. Lumpkin, J. Nucl. Mater. 289 (2001) 136.
[18] M. Lang, J. Lian, J.M. Zhang, F.X. Zhang, W.J. Weber, C. Trautmann, R.C. Ewing, Phys. Rev. B (Conden. Mat. Mater. Phys.) 79 (2009) 224105.
[19] G. Sattonnay, S. Moll, M. Herbst-Ghysel, C. Legros, J.-M. Costantini, L. Thomé, Nucl. Instrum. Meth. Phys. Res. B 266 (2008) 3052.
[20] Y. Zhang, I. -T Bae, W.J. Weber, Nucl. Instrum. Meth. Phys. Res. B 266 (2008) 2828.
[21] G. Sattonnay, S. Moll, L. Thomé, C. Legros, M. Herbst-Ghysel, F. Garrido, J.-M. Costantini, C. Trautmann, Nucl. Instrum. Meth. Phys. Res. B 266 (2008) 3043.
[22] Y. Zhang, W.J. Weber, V. Shutthanandan, R. Devanathan, S. Thevuthasan, G. Balakrishnan, D.M. Paul, J. Appl. Phys. 95 (2004) 2866.
[23] Y. Zhang, V. Shutthanandan, R. Devanathan, S. Thevuthasan, D.E. McCready, J. Young, G. Balakrishnan, D.M. Paul, W.J. Weber, Nucl. Instrum. Meth. Phys. Res. B 218 (2004) 89.
[24] R.C. Ewing, L.M. Wang, Nucl. Instrum. Meth. Phys. Res. B 65 (1992) 319.
[25] S.X. Wang, L.M. Wang, R.C. Ewing, G.S. Was, G.R. Lumpkin, Nucl. Instrum. Meth. Phys. Res. B 148 (1999) 704.
[26] S.X. Wang, L.M. Wang, R.C. Ewing, K.V. Govidan Kutty, in: S.J. Zinkle, G.E. Lucas, R.C. Ewing, J.S. Williams (Eds.), Microstructural Processes in Irradiated Materials, Mater. Res. Soc. Symp. Proc. 540 (1999) 355.
[27] W.J. Weber, N.J. Hess, Nucl. Instrum. Meth. Phys. Res. B 80–81 (1993) 1245.
[28] J. Lian, L. Wang, J. Chen, K. Sun, R.C. Ewing, J. Matt Farmer, L.A. Boatner, Acta Mater. 51 (2003) 1493.
[29] G. Balakrishnan, O.A. Petrenko, M.R. Lees, D.M. Paul, J. Phys. Condens. Mat. 10 (1998) L723–L725.
[30] James F. Ziegler, Jochen P. Biersack, Matthias D. Ziegler, The Stopping and Range of Ions in Solids, SRIM Co., 2008. as well as the orginal book of by J.F. Ziegler, J.P. Biersack, and U. Littmark, (Pergamon, New York, 1985).
[31] Y. Zhang, W.J. Weber, V. Shutthanandan, S. Thevuthasan, Nucl. Instrum. Meth. Phys. Res. B 251 (2006) 127.
[32] Y. Zhang, Z. Zhu, W.D. Bennett, L.V. Saraf, J.L. Rausch, C.A. Hendricks, W.J. Weber, J. Lian, R.C. Ewing, J. Nucl. Mater. 389 (2009) 303.
[33] L.C. Feldman, J.W. Mayer, S.T. Picraux, Materials Analysis by Ion Channeling, Academic Press, New York, 1982. pp. 117.
[34] M.L. Swanson, in: J.R. Tesmer, M. Nastasi (Eds.), Handbook of Modern Ion Beam Materials Analysis, Materials Research Society, Pittsburgh, PA, 1995, p. 263.
[35] J.S. Williams, R.G. Elliman, in: J.R. Bird, J.S. Williams (Eds.), Ion Beams for Materials Analysis, Academic Press, Australia, 1989, p. 286.
[36] Y. Zhang, W.J. Weber, Appl. Phys. Lett. 83 (2003) 1665.
[37] Y. Zhang, William J. Weber, Nucl. Instrum. Methods Phys. Res. B 267 (2009) 1705.
[38] Y. Zhang, J. Jensen, G. Possnert, D.A. Grove, I.-T. Bae, W.J. Weber, Nucl Instrum. Meth. B 261 (2007) 1180.
[39] Y. Zhang, W.J. Weber, D.E. McCready, D.A. Grove, J. Jensen, G. Possnert, Appl. Phys. Lett. 87 (2005) 104103.
[40] Y. Zhang, W.J. Weber, D.A. Grove, J. Jensen, G. Possnert, Nucl. Instrum. Meth. B 250 (2006) 62.
[41] Y. Zhang, J. Jensen, G. Possnert, D.A. Grove, D.E. McCready, B.W. Arey, W.J. Weber, Nucl. Instrum. Meth. B 249 (2006) 18.
[42] L. Nowicki, A. Turos, R. Ratajczak, A. Stonert, F. Garrido, Nucl. Instrum. Meth. B 240 (2005) 277.
[43] S. Moll, L. Thomé, L. Vincent, F. Garrido, G. Sattonnay, T. Thomé, J. Jagielski, J-M. Costantini, J. Appl. Phys. 105 (2009) 023512.
[44] W.J. Weber, Nucl. Instrum. Methods Phys. Res. B 166–167 (2000) 98.
[45] Y. Zhang, J. Lian, C.M. Wang, W. Jiang, R.C. Ewing, W.J. Weber, Phys. Rev. B 72 (2005) 094112.
[46] Y. Zhang, W.J. Weber, W. Jiang, A. Hallén, G. Possnert, J. Appl. Phys. 91 (2002) 6388.
[47] Y. Zhang, W.J. Weber, W. Jiang, C.M. Wang, V. Shutthanandan, A. Hallén, J. Appl. Phys. 95 (2004) 4012.
[48] F.L. Vook, H.J. Stein, Radiat. Eff. 2 (1969) 23.
[49] W.J. Weber, J. Nucl. Mater. 98 (1981) 206.